Chemical Engineering Journal 155 (2009) 457–465

Contents lists available at ScienceDirect

Chemical Engineering Journal

journal homepage: www.elsevier.com/locate/cej

Influence of process parameters on microcapsules loaded with *n*-hexadecane prepared by *in situ* polymerization

F. Salaün[a,b,*], E. Devaux[a,b], S. Bourbigot[a,c], P. Rumeau[d]

[a] *Univ Lille Nord de France, F-59000 Lille, France*
[b] *ENSAIT, GEMTEX, F-59100 Roubaix, France*
[c] *ENSCL, PERF, F-59650 Villeneuve d'Ascq, France*
[d] *IFTH, F-69134 Ecully, France*

ARTICLE INFO

Article history:
Received 20 April 2009
Received in revised form 26 June 2009
Accepted 2 July 2009

Keywords:
Amino resin
Microencapsulation
Emulsion
Droplet size
Surface tension

ABSTRACT

A series of melamine–formaldehyde microcapsules containing *n*-hexadecane were synthesized by *in situ* polymerization from partial etherified melamine–formaldehyde resins. This research was conducted to clarify the influence of different parameters on the encapsulation process, i.e. during the emulsion formation step and during the shell formation using surface tension measurement, Fourier-transform infrared spectroscopy and differential scanning calorimetry. By carefully analyzing the influencing factors including phase volume ratio, types of surfactants and content, stirring rate and time, pH, reaction time, feeding weight ratio of core/shell pre-polymer, the optimum synthetic conditions were found out. The results indicated that a binary mixture of Tween-20 and Brij-35 was found suitable emulsifier at low pH. Furthermore, formaldehyde/melamine (F/M) mole ratio influenced not only the shell formation mechanism but also the particle size distribution, microcapsule morphology and resin conversion rate.

1. Introduction

A variety of available phase change materials (PCMs) are well-known for their thermal characteristics. During their phase change stage, these compounds can absorb or release the latent heat while the temperature of the material is kept constant. One of the trend of this two past decades is microencapsulated PCM, which provides enhanced thermal insulation in a wide variety of applications [1–3]. To improve thermal protective clothing, the PCMs used for this technology are carbohydrates with different chain lengths [4,5] or aliphatic hydrocarbon compounds [6,7], whose phase change takes place in a temperature range close to the human skin's one.

One of the most typical methods which may be used to microencapsulate a PCM is to disperse droplets of this molten material in an aqueous solution and to form walls around the droplets using techniques such as phase coacervation, interfacial polymerization and *in situ* polymerization. Microencapsulated PCMs have been synthesized with gelatin by coacervation [8], polyamide [9], polyurethane or polyurea [10,11] by interfacial polymerization, urea–formaldehyde, urea–resorcinol–formaldehyde [12], and melamine–formaldehyde (MF) [13,14] by *in situ* polymerization.

The use of MF resin has attracted many researchers to improve the thermal stability of microencapsulated PCMs [15]. Furthermore, melamine–formaldehyde pre-polymers offer some advantages to the synthesis of microcapsules due to their high reactivity, and therefore a short reaction time and a controlled amount of polymer to form the shell with a high loading content.

A two step microencapsulation process has been studied. The first step is the liquid–liquid dispersion and the second step is the microencapsulation by *in situ* polymerization. In the preparation of microencapsulated PCMs by an *in situ* polymerization, the dispersion of *n*-alkane in the continuous phase is the determining step in establishing the size distribution of the final microcapsule. However, to control the morphology and to prepare the microcapsules having the desired physical properties, it is necessary to know the membrane forming mechanism. The dispersion of the organic phase in the continuous aqueous phase is affected to a great extent by the physicochemical properties of the two immiscible phases as well as by the characteristics of the agitation system. Variations in these physical and design parameters influence the size distribution of the dispersed organic phase. It is thus essential that the dispersed liquid droplets are sized for a period of time before the formation of the capsules' polymer wall. So, a well-controlled microencapsulation process should typically lead to the production of microcapsules having a narrow capsule

* Corresponding author at: ENSAIT, GEMTEX, F-59100 Roubaix, France. Tel.: +33 3 20 25 64 59; fax: +33 3 20 27 25 97.
E-mail address: fabien.salaun@ensait.fr (F. Salaün).

1385-8947/$ – see front matter © 2009 Elsevier B.V. All rights reserved.
doi:10.1016/j.cej.2009.07.018

Table 1
Formulation of melamine–formaldehyde microcapsule. Influence of the type of pre-polymer and emulsion parameters.

Sample code[a]	Amount of pre-polymer (g)	*n*-Hexadecane (g)	Water (g)	pH adjustment at 4		Continuous phase viscosity[b] (mPa s)	Stirring rate (rpm)	ΔH_m[c] (J g^{-1})	*n*-Hexadecane content[d]	
				Emulsion	Encapsulation				Measured (wt.%)	Theoretical (wt.%)
$M_{5.6}$FMe-1	17.5	10	57.5		X		13500			
$M_{5.6}$FMe-2	17.5	10	57.5	X	X		13500			
$M_{5.6}$FMe-3	17.5	10	57.5	X	X	8	9500	111	47.8	36.4
$M_{5.6}$FMe-4	8.75	10	66.25	X	X	1.5–1.8	9500	156	67.2	53.3
$M_{5.6}$FMe-5	25.2	10	49.3	X	X	14	9500	84	36.2	28.4
$M_{5.6}$FMe-6	50.4	10	24.6	X	X	50	9500	44	18.9	16.5
M_4FMe-1	50.4	10	24.6	X	X		9500			
M_6FMe-1	50.4	10	24.6	X	X		9500			

[a] M represents the melamine, F the formaldehyde, Me the methanol and the subscript is the molar ratio of formaldehyde per melamine.
[b] Brookfield viscosity at 45 °C and 20 rpm.
[c] ΔH_m: melting enthalpy of microcapsule.
[d] Calculated from Eq. (6).

size distribution. On the one hand, experiments were conducted to characterize the influence of parameters governing the emulsion step. On the other hand, the effect of melamine–formaldehyde pre-polymer on the membrane formation mechanism was investigated.

2. Experimental

2.1. Materials

n-Hexadecane (C16) with purity grade of 99.4% was employed as lipophilic phase to be a core material. A melamine–formaldehyde resin partially etherified with methanol from melamine and formaldehyde (37 wt.%) purchased from Acros Organics was used to prepare the wall materials. The polyoxyethylene (20) sorbitan monolaurate (i.e. Tween-20 or Tw-20) and polyoxyethylene (23) lauryl ether (i.e. Brij-35 or B-35), obtained from Acros Organics were employed as surfactant. Citric acid, sodium hydroxide, sulfuric acid and triethanolamine obtained from Aldrich (France) as pH control agents were used without any further purification prior to use.

2.2. Preparation of microcapsules

The microencapsulation of *n*-hexadecane was carried out in a 250 ml three neck round-bottomed flask equipped with a mechanical stirrer via an *in situ* polymerization. The preparation conditions and the corresponding adopted nomenclature are summarized in Table 1.

- Preparation of MF resin pre-polymer
  81 ml of a formaldehyde solution (37%) were adjusted to pH 9 in 500 ml three necked flask equipped with a hook stirrer and a condenser by adding 10 wt.% NaOH aqueous solution at 80 °C. After adding 21 g of melamine, a clear solution was formed, the heating was continued until the boiling started. After cooling down to 62 °C, pH was reduced to 1 by adding a solution of sulfuric acid (10.0 wt.%). When the contents had acquired a milky turbid appearance, 76 ml of methanol were added. Thus, a proportion of the hydroxymethyl groups were reacted with the primary alcohol to form the corresponding ether. The contents of the flask were cooled to 40 °C in the course of 1 h. After the end of etherification, the mixture was neutralized with a requested amount of triethanolamine and the excess alcohol was distilled off (Fig. 1a). Thus, M_6FMe pre-polymer was obtained. To synthesize $M_{5.6}$FMe and M_4FMe resin, 76 and 54 ml of formaldehyde solution were employed to react with melamine, respectively (where M represents the melamine, F the formaldehyde, Me the methanol and the subscript is the molar ratio of formaldehyde per melamine).
- Emulsion step
  n-Hexadecane was added into an aqueous solution of melamine–formaldehyde pre-polymer and surfactant. This mixture was vigorously dispersed by a homogenizer (ultra turrax high speed homogenizer (Ika T 25 basic, Germany)) at 45 °C at a selected rate (Table 1).
- Shell formation
  The emulsion was adjusted to pH 4 with 10.0 wt.% citric acid solution. The stirring speed was decreased to 300 rpm after 20 min. Polymerization of melamine–formaldehyde and microencapsulation were attained with continuous agitation for 4 h at 55 °C. Then, the pH of the solution was adjusted to 9 with 50 wt.% triethanolamine solution to complete the reaction (Fig. 1b). The suspension was cooled to 25 °C and filtered, the microcapsules were washed twice with methanol and distilled water, and dried in a vacuum oven.

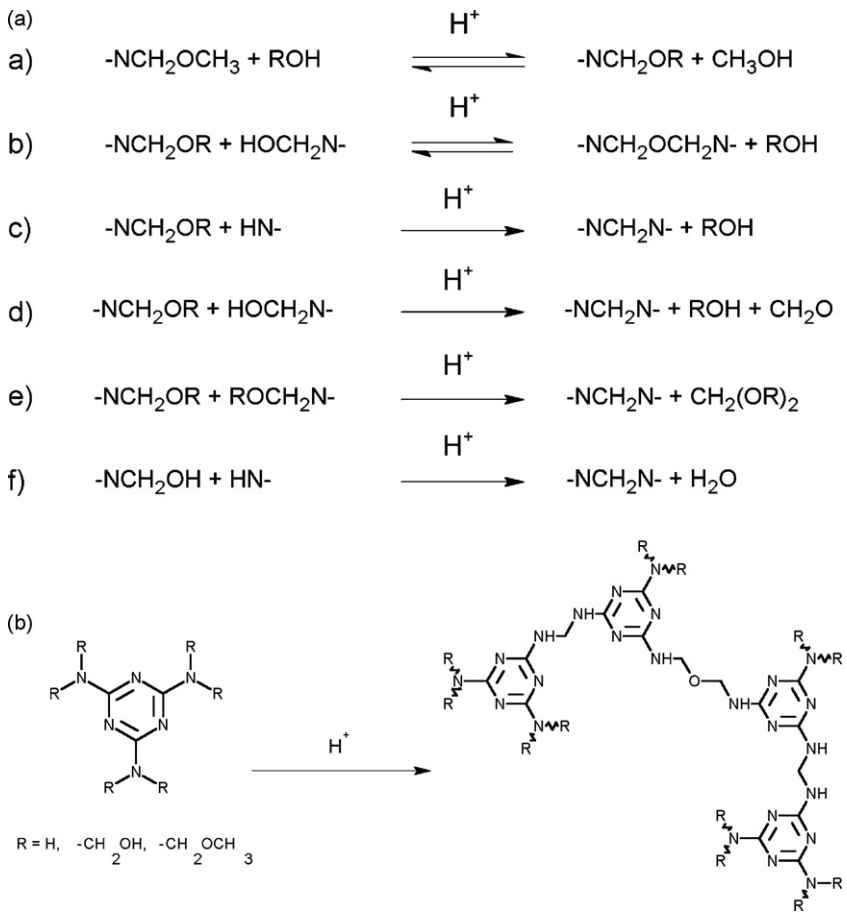

Fig. 1. Reaction schemes of melamine–formaldehyde resin. (a) Formation of melamine–formaldehyde pre-polymer. (b) Formation of cross-linked melamine–formaldehyde.

2.3. Analytical methods

2.3.1. Tensiometry

Surface tensions of the various liquids and the interfacial tension between *n*-hexadecane and continuous phase (water and water + amino resin + Tween-20) were performed at 20 °C by a ring tensiometer (Prolabo TD 2000 tensiometer) according to the ASTM C1331 and D0971, respectively. The vessel was washed with detergent, placed in chromosulfuric acid overnight, washed with distilled water, and briefly flamed with a Bunsen burner prior to use. The platinum ring was rinsed in acetone and distilled water, and flame before use. The Zuidema–Waters method was employed for the ring correction.

The concentrated surfactant solution in water was progressively added with the help of a microsyringe and measurement of surface tension after proper mixing and equilibration at a constant temperature was realized. The accuracy of measurement was ±0.1 mN m^{-1}. The measurements were duplicated and the mean values were considered for analysis. Area/molecule was calculated using the Gibbs adsorption equation:

$$\Gamma = -\frac{1}{RT}\left(\frac{\mathrm{d}\gamma}{\mathrm{d}(\ln C)}\right) \quad (1)$$

where Γ is the surface concentration of surfactant in the solution, γ is surface tension at equilibrium (mN m^{-1}) of a surfactant solution of concentration C (mol l^{-1}), R is the universal gas constant (8.314×10^{-3} kJ mol^{-1} K^{-1}), T is the temperature (K) and $\mathrm{d}\gamma/\mathrm{d}(\ln C)$ is the slope of the straight line before CMC (critical micelle concentration) value.

The average area per molecule (A) occupied by one compound molecule in the surface layer (assuming the layer is monomolecular) can be obtained from the equation:

$$A = \frac{1}{N_A \Gamma} \quad (2)$$

where N_A is the Avogadro's number.

The standard free energy of micellization of individual surfactants was calculated by the relation:

$$\Delta G^{\circ}_{\mathrm{m}} = RT \ln \mathrm{CMC} \quad (3)$$

The nature and extent of the interaction between the two different surfactant molecules can be measured by the molecular interaction parameters β. Negative β values indicate attractive interaction and positive values, repulsive interaction. The molecular interaction parameter for mixed adsorption film formation at the air/water interface using the equation derived by Rubingh [18] and Rosen [19] can be expressed as follows:

$$\beta = \frac{\ln(\alpha C_{12}/X_1 C_1)}{(1-X_1)^2} \quad (4)$$

where α is the mole fraction of surfactant 1 in the mixture of two surfactants, X_1 is the molar fraction of surfactant 1 in the total surfactant in the mixed micelle; C_1, and C_{12} are the critical micelle concentrations of surfactants 1 and the binary mixture, respectively, at a given value of α. X_1 can be determined by solving iteratively the following relationship:

$$\frac{(X_1)^2 \ln(\alpha C_{12}/X_1 C_1)}{(1-X_1)^2 \ln\left[(1-\alpha)C_{12}/(1-X_1)C_2\right]} = 1 \quad (5)$$

Table 2
Interfacial and thermodynamical behaviors of pure and binary mixture of Tween-20 and Brij-35 at 298 K.

$\alpha_{\text{Tween-20}}$	CMC	X_1	β	Γ (10^6 mol m^{-2})	A (nm^2)	ΔG_m° (kJ mol^{-1})
0.00	9.12E−05			4.65	0.354	−34.46
0.25	8.07E−05	0.336	−0.006	4.42	0.372	−34.76
0.40	7.56E−05	0.504	−0.014	5.27	0.312	−34.92
0.50	7.19E−05	0.603	−0.062	5.71	0.288	−35.05
0.70	6.70E−05	0.780	−0.025	5.64	0.292	−35.22
0.80	6.46E−05	0.859	−0.031	6.03	0.273	−35.31
0.90	6.23E−05	0.932	−0.047	6.46	0.255	−35.40
1.00	6.02E−05			6.73	0.244	−35.49

2.3.2. Particle size analysis

Particle diameters were obtained with a laser-light blocking technique (AccusizerTM, model 770, Particle sizing systems, Santa Barbara, CA, and C770 software version 2.54). The particle size distribution was constructed one particle at a time, by comparing the detected pulse heights with standard calibration curve, obtained from a set of uniform particles of known diameter. Measurements were performed in triplicate at room temperature. Data obtained were expressed as the mean particle diameter. All particle size measurements were repeated 3 times per sample and each sample was prepared in triplicate. The average values and standard deviations were calculated.

2.3.3. Morphology of the particles

The microscopic aspects of the particles were observed by both optical microscopy (Axioskos Zeiss) equipped with a camera (IVC 800 12S) and scanning electron microscopy (Philips XL30 ESEM/EDAX – SAPPHIRE).

2.3.4. Infrared spectroscopy

The structure of the shell polymer was analyzed by FT-IR spectra. Samples were ground and mixed with KBr to make pellets. FT-IR spectra in the transmittance mode were recorded using a Nicolet Nexus, connected to a PC, in which the number of scan was 128 and the resolution was 4 cm^{-1}.

2.3.5. Differential scanning calorimetry

The thermal behavior of *n*-hexadecane and the particles was recorded using a TA instrument type DSC 2920 piloted on PC with TA Advantage control software. The sample space was purged with nitrogen at a constant flow (50 ml min^{-1}) during the experiments. Transition temperatures and enthalpies were obtained from a least four independent experiments with a scanning speed of 2 K min^{-1}. The weight of all samples was kept in approximately 4 mg. The specific heat of *n*-hexadecane was a constant in the measured temperature range. The content of *n*-hexadecane in the microcapsules can be estimated according to the measured enthalpy:

$$n\text{-Hexadecane content} = \frac{\Delta H_{\text{microcapsules}}}{\Delta H_{n\text{-hexadecane}}} \times 100\% \quad (6)$$

where $\Delta H_{\text{microcapsules}}$ and $\Delta H_{n\text{-hexadecane}}$ are the melting enthalpy of microcapsules and *n*-hexadecane (232 J g^{-1}), respectively.

3. Result and discussion

The manufacture of microcapsules was carried out by using an *in situ* polymerization technique. The process includes two main steps, e.g. emulsification step which determines the size and the size distribution of the microcapsules; and the formation of the capsules. The emulsification step may be influenced at once by physical parameters such as apparatus configuration, stirring rate and volume ratio of the two phases, and by physicochemical properties such as interfacial tension, viscosities, densities and the chemical compositions of the two phases. The second step is governed by the ability of amino resins for self-condensation around the core material droplet which is linked to its surface activity and is an enrichment of resin molecules within the interface. Each step was keenly observed to understand the effect on the particle size and the formation mechanism of the shell. Thus, to determine the optimal conditions for the synthesis of melamine–formaldehyde microcapsules containing *n*-hexadecane, the effects of the molar ratio *R* (melamine to formaldehyde), the type of the organic phase, the type and the amount of the surfactant, the pH and the reaction time were investigated in this work.

3.1. Formulation of the emulsion

3.1.1. Surfactants selection

The formation of microcapsules is greatly affected by the surfactant, which influences not only the mean diameter but also the stability of the dispersion. The surfactants used in the system has two roles, one to reduce interfacial tension between oil and aqueous phases allowing formation of smaller microcapsules and one to prevent coalescence by its adsorption on the oil–water interface and therefore by forming a layer around the oil droplets.

In order to find out optimum conditions for the emulsification step, two kinds of surfactants were used to prepare the emulsion and their effects on the characteristics of the above step were investigated. The surfactant used in this study, Tween-20 and Brij-35, have a hydrocarbon tail consisting of 12 carbon atoms and a head group consisting of 20 and 23 ethylene oxide residues, respectively (Fig. 2). Surfactant molecules are usually adsorbed at the air–water interface and this adsorption results in the surface tension reduction.

Table 2 summarizes the CMC and adsorption parameters at the water–air interface of the various formulations. The CMC values at 25 °C for pure surfactants, i.e. Tween-20 (6.02E−05 M) and Brij-35 (9.12E−05 M) are in good agreement with the literature values [16,17]. The critical micelle concentrations of the mixed surfac-

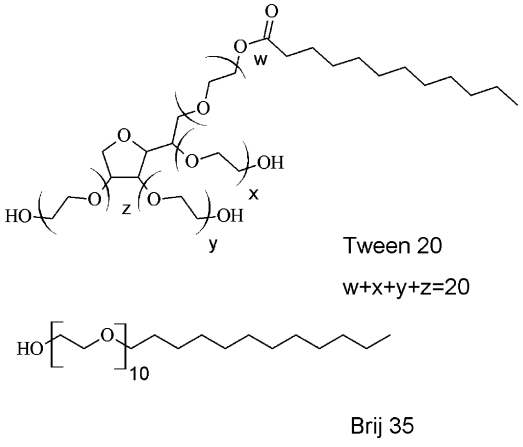

Fig. 2. Structures of Tween-20 and Brij-35.

tants system varied with the relative amount of mole surfactants. Mixed surfactant systems are much favored since they often provide better performance than pure surfactants. This finding is in agreement with early studies which revealed that in the mixed nonionic–nonionic surfactants systems, the mean head size in an organized assembly would become rather small. This was due to the minor structural difference between the head group of Tween-20 and Brij-35 has resulted weak attractive interaction.

The adsorption parameters values were determined on the basis of the adsorption isotherms using the Gibbs equation for nonionic surfactants. The surface area per molecule (A) of the nonionic surfactants (Tween-20, 20 EO and Brij-35, 23 EO) increases with the number of ethoxy units (EO) which are the polar head. Thus, less Brij-35 molecules are necessary to saturate the interface (Γ). The micellar compositions (X) of Tween-20 in the binary mixture are slightly higher than the stoichiometric composition and the mutual interaction parameter (β) values are negative, which suggests a minor synergism. Furthermore, it is seen that from examination of the thermodynamic parameters (Table 2), the standard free energy of micellization ΔG_m° becomes less negative with the increase in concentration of Brij-35 in the mixture. Thus, the values of ΔG_m° were found to be negative indicating synergistic interaction at the interface. The A value is lower in mixed surfactant systems at certain bulk concentrations and no regular trends were observed.

3.1.2. Effect of the pH of aqueous phase

The surface activity of surfactants is related to the manner in which molecules align at an interface. Thus, the orientation of surfactant molecules at the interfaces is important to determine the dynamic and equilibrium properties of the system. Additional investigations on the influence of pH on the surface tension were performed to elucidate the surface forces governing the stabilization of the droplets during the emulsification step with increasing nonionic surfactant concentration (Fig. 3). In the scientific literature about the preparation methods of amino resin microcapsules, the pH of the reaction mixture was adjusted at the beginning of the reaction after the emulsion step. In our study, surface tension of aqueous phase was studied at various pH values of the solution. It was found that the surface tension reached a minimum value related to the pKa values of the citric acid as shown in Fig. 3. This

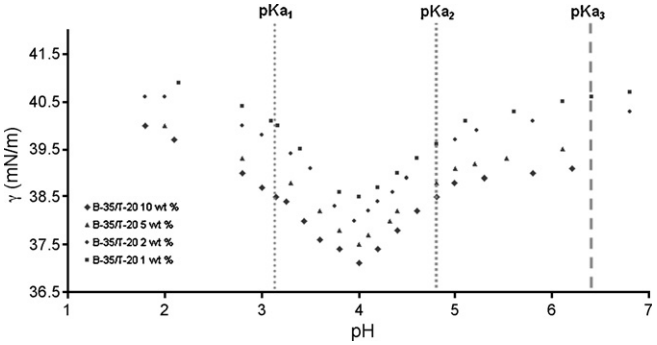

Fig. 3. Effect of pH on the surface tension of the aqueous phase.

figure indicates also that the surface tension decreases with pH increasing between 2 and 4, and increases with pH above 4. The surface tension was reduced for a value of pH near $(pKa_1 + pKa_2)/2$. The decrease in surface tension upon addition of citric acid to the surfactant solution could be explained by the interaction between citric acid and surfactants in the water.

Thus, this fact indicates that the cooperation among molecules at interfaces (induced by the van der Waals interactions between chains and the polar interactions) causes reduced intermolecular distances leading to influence the performance of the emulsification. It was shown previously [20] that a subangstrom change in intermolecular distance can be produced by the ionization of the polar head groups near to their pKa values, in the case of a fatty acid.

3.1.3. Effect of phase volume ratio

Particle formation during the homogenization depends on a stress balance between the turbulent forces tending to break up the droplet and the forces from interfacial tension holding a droplet together [21]. The degree of a liquid droplet break-up is led by three forces as surface tension that tries to maintain the spherical shape while viscous and inertial forces attempt to deform the droplet. The droplet size is determined by a balance between the droplet break-up and the coalescence forces. These two factors are considered to be the most important phenomena determining the droplet size

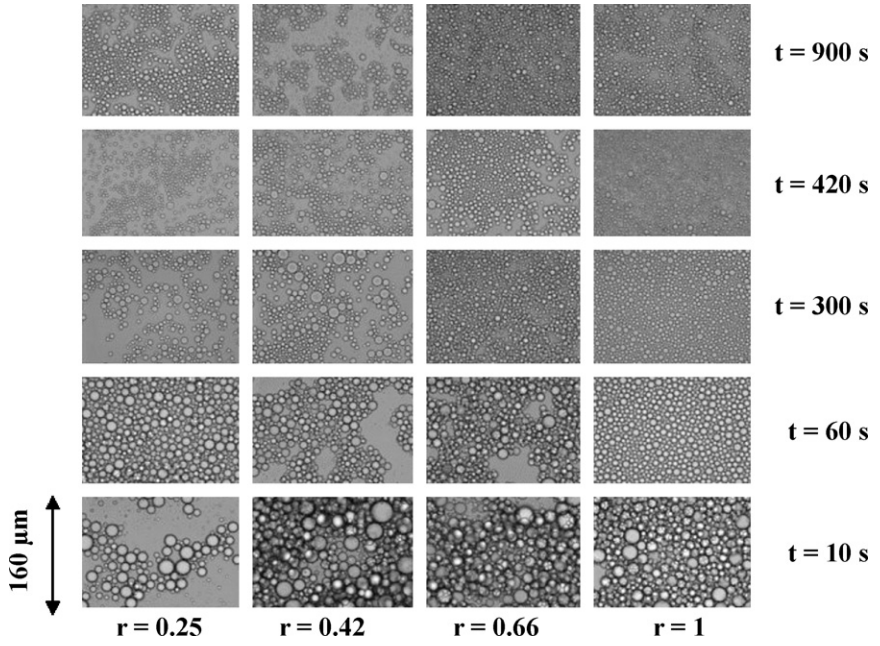

Fig. 4. Effect of organic/aqueous phase ratio on the properties of the emulsion.

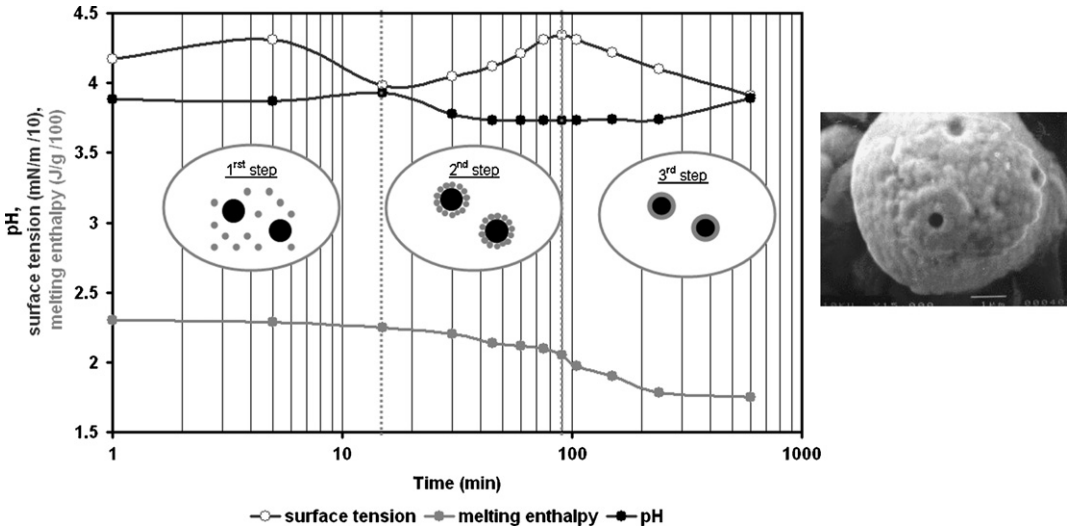

Fig. 5. pH, surface tension and melting enthalpy profiles during microencapsulation.

and size distribution in emulsification process. The effect of the volume ratio between the dispersed phase and the continuous phase is shown in Fig. 4. Emulsions of four ratios were prepared by homogenization at 8000 rpm using a rotor/stator apparatus. As seen in Fig. 4, an identical equilibrium emulsion droplet size was obtained in all cases after 15 min. Furthermore, the time duration to obtain a narrow particle size distribution decreases with the increasing of the volume ratio. After storage at room temperature, a creaming phenomenon of the droplets was observed, related to the difference in density between the two phases. The higher the volume ratio is, the faster the bursting speed is. The latter varies from 10 min for $r = 0.25$ to a few hours for $r = 1$. After a day, all the solutions are separated in two phases where the lower phase is a paraffin microemulsion in the water formed by the satellite micro-droplets whereas the higher phase is mainly made up of larger paraffin droplets in suspension in the aqueous phase. Emulsions composed of droplets in the micron-size range are not thermodynamically stable and there are various sources of instability leading ultimately phase separation. Creaming or sedimentation of droplets can occur depending on the density difference between the dispersed and continuous phase and can be enhanced or restricted by flocculation. During the phase separation, since large and small droplets can become deformable under low interfacial tension, inter-droplet attraction occurs and enhances coalescence and creaming [22]. After 24 h, no variation of the mean droplet size was observed for low r, whereas for $r = 0.66$ and $r = 1$ coalescence has taken place. The above results indicate that the stability of emulsion was significantly depended on the r value and the storage time. Thus, when r increases, the probability for the dispersed micelles to coalesce for forming large droplet should be increased, therefore the stability of the *n*-hexadecane droplet is enhanced with low r value. So, for the second part of the work a r value of 0.42 was chosen.

3.2. Shell microcapsule formation

3.2.1. Mechanism of shell formation

The melamine–formaldehyde shell is synthesized on the surface of the droplets of *n*-hexadecane via an *in situ* polymerization between the melamine–formaldehyde pre-polymers, which occurs under an acidic condition. The thermostability and the structure of the produced microcapsules depend on the molar ratio of melamine/formaldehyde. Thus, the cross-linking degree is increased with high amount of formaldehyde since it leads to greater amount of hydroxymethyl precondensate, whereas smaller amount of formaldehyde induces lower cross-linking degree [23]. In the melamine–formaldehyde pre-polymer, according to the substitution by formaldehyde, the amidogen hydrogens of melamine were partially or completely displaced by methylol (Fig. 1a). In this study, pH and surface tension were monitored during a standard microencapsulation process; and powder recovered from the sample taken off was analyzed by DSC to determine the reaction time allowing to obtain a solid shell, e.g. to maintain entrapped the core material (Fig. 5).

The formation of the microcapsule shell occurs in three consecutive stages. After the addition of citric acid solution to adjust the pH to 4, the solution temperature is increased slowly. During the first 20 min, the melamine–formaldehyde pre-polymers obtain H^+ changing into active pre-polymers, then the degree of etherification increases, due to a reduction in hydroxyl group concentration (Fig. 1a and b). Thus, the modification of surface tension observed in Fig. 5 corresponds to a decrease of the water solubility of the pre-polymer since the polymeric material separates from the continuous phase as a liquid solution relatively concentrated in active pre-polymer. In the second stage observed in the time range of 20–90 min, surface tension sharply increases as pH decreases, and this was also accompanied by the decrease of melting enthalpy of the recovered sample. The modification of the surface tension is linked to the ability of amino resins to wet the core material droplet to create primary shell around the dispersed *n*-hexadecane. The concentration of resin in the boundary layer is enhanced by the hydrophilic/hydrophobic interactions of the partial methylolated melamine, and therefore to an enrichment of resin molecules within the interface [24]. From this stage, it is possible to recover particle under powder form, nevertheless the capsule walls are not yet stable and not completely harden, because the particles collapse during drying. Even if the microcapsules can be observed using microscopy, they are easily destroyed or deformed if the agitation is stopped, since the thickness of the shell is too small to allow a completed entrapment of the core material. In the last stage, from 90 to 600 min, since amino resin pre-polymer is enriched at the interface as shown in Fig. 5 with the decrease of the surface tension, the reaction rate of the polycondensation at the interface is increased with the result of microcapsule shell formation. According to Dietrich et al. [25], the formation of capsule wall is only possible if the polycondensation rate at the phase boundary is higher than in aqueous dispersion medium. Therefore, the resin condensation proceeds much faster in the boundary layer than in the volume phase, allowing the formation of tougher capsule walls. The more the poly-

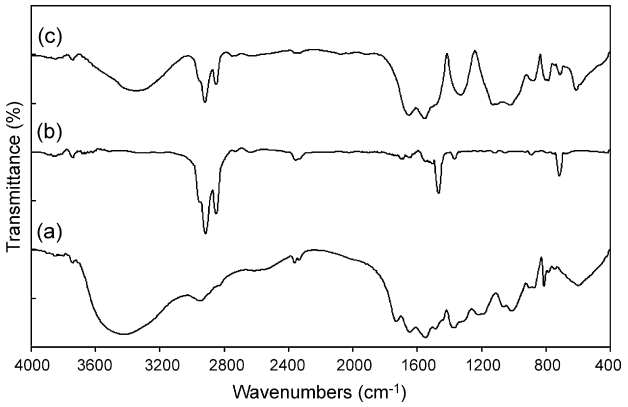

Fig. 6. FT-IR spectra of shell polymer (a), *n*-hexadecane (b) and microcapsules (c).

condensation occurs the more the surface becomes hydrophobic and the more the surface tension decreases, since the pre-polymer was cross-linked either by ether linkage or methylene as shown in Fig. 1b. The shell of the microcapsules becomes thick owing to the further reaction of pre-polymer and from 240 min, no melting enthalpy variation was observed, indicating that the reaction was completed. Furthermore, the microcapsules shown in Fig. 5 present a rough surface with smaller particles with a diameter of 0.2 μm which look like melamine–formaldehyde nanoparticles. In this experiment, this rough surface suggests the formation of tiny particles of melamine–formaldehyde pre-polymer which tend to deposit onto the *n*-hexadecane droplet surface previously to their cross-linking to form a solid hard shell. Furthermore, drying process can also results in the rough surface of microcapsules.

3.2.2. Structure of microcapsules

The FT-IR spectra of *n*-hexadecane, melamine–formaldehyde shell and microcapsules are presented in Fig. 6 to allow the identification of various core and shell microcapsules via known characteristic wavenumbers. As seen in the figure, the spectra (b) and (c) show a strong absorption band at 2920–2852 cm^{-1} associated with the aliphatic C–H stretching vibrations of the *n*-hexadecane. The in-plane rocking vibration of the CH_2 groups is observed at 717 cm^{-1}, and C–H bending vibration in CH_2 is found at 1470 and 1370 cm^{-1}. Characteristic broad band responsible for hydroxyl, imino and amino stretching were observed around 3420 cm^{-1} in the spectrum of the microcapsule shell (Fig. 6a). Alkyl C–H stretching vibration was found around 2950 cm^{-1}. The C–N multiple stretchings in the triazine ring are observed at 1550 and 1488 cm^{-1}. C–H bending vibration in CH_2 was found at 1490 and 1373 cm^{-1} due to methylene bridges. The characteristic absorption bands of aliphatic C–N vibration appeared between 1200 and 1170 cm^{-1}. Characteristic triazine ring bending at 810 cm^{-1} can also be observed. C–O–C stretching due to ether bridge at 1060 cm^{-1} is also present. All of the characteristic peaks for *n*-hexadecane and amino resin can be clearly distinguished in the spectra of the FT-IR spectrum of the microcapsule samples, which verifies that *n*-hexadecane has been successfully encapsulated by melamine–formaldehyde resin.

3.2.3. Effects of stirring time and stirring rate

The effects of stirring rate and time on the size distribution are depicted in Table 3. In the microencapsulation process, the determinant step in establishing the mean diameter or the size distribution of the microcapsules is the emulsification process. The emulsification of the organic phase in the aqueous phase is significantly affected by the physicochemical properties of the two immiscible phases, and also by the shearing system. In the present

Table 3
Mean diameter and standard deviation of microcapsules as a function of the stirring rate and stirring time for samples prepared from M_4FMe-1.

Stirring time (min)	Stirring rate (rpm)			
	6500	9500	13500	17500
5	3.4 ± 5.2	2.4 ± 3.2	2.2 ± 2.8	1.6 ± 2.5
10	2.3 ± 3.9	2.1 ± 2.6	2.1 ± 2.6	1.4 ± 3.2
15	1.9 ± 2.8	1.8 ± 3.2	1.8 ± 2.4	1.3 ± 2.0
20	1.6 ± 2.5	1.5 ± 2.8	1.6 ± 2.0	1.2 ± 1.5
30	1.5 ± 1.5	1.4 ± 1.8	1.3 ± 1.7	1.1 ± 1.1

work, the effects of the type of rotational speed and time were investigated. In both of cases, the obtained microcapsules have a relatively monomodal size distribution. As a result, the average size is decreased and their size distribution becomes narrow when the stirring rate and the duration of the stirring are increased [24]. Higher stirring speeds increase the rate of the droplet breakage due to the increased turbulent energy acting on the surface of the droplet. As seen in Table 3, an identical equilibrium microcapsule size about 1.6 μm is obtained for 6500, 9500 and 13500 rpm and 1.2 μm for 13500 rpm after 20 min.

Furthermore, according to the kind of pre-polymer used to encapsulate the *n*-hexadecane, the effect of the stirring may be more pronounced. Thus, in the case of $M_{5.6}$FMe, the analysis of the size distributions (Fig. 7) shows that the microcapsules are multi-dispersed with a wide particle size distribution between 1 and 10 μm. With a stirring rate of 13500 rpm, the size distribution curve reaches a maximum around 2 μm, whereas the maximum appears at 7 μm for 9500 rpm. It is worth noting that these syntheses show a small peak at about 600 nm. As seen in Fig. 8, this latter shows the presence of nanoparticles of melamine–formaldehyde resins.

In the previous part, we showed that the pH establishment of the amino resin during the emulsion step tends to stabilize the emulsion via intermolecular interactions. Furthermore, as underlined by Dietrich et al. [25] melamine–formaldehyde precondensates exhibit surface activity due to their molecular structure possessing both hydrophobic and hydrophilic groups. Thus, when the amino resin is incorporated during this step and pH adjusted to 4, the primary membrane formation may occur at the same time as the break-up process and deformation mechanisms of the droplet under high shear rate. Therefore, a decrease in average diameter and size distribution are observed as shown in Fig. 9a and b. In fact, the low pH catalyses the polycondensation of amino pre-polymer and promotes the formation of small MF particles which tend to deposit on the surface of microcapsules. As mentioned by Lee et al. [26], the low pH promotes the formation of methylene bridges affecting the amino resin solubility and therefore the surface morphology. The

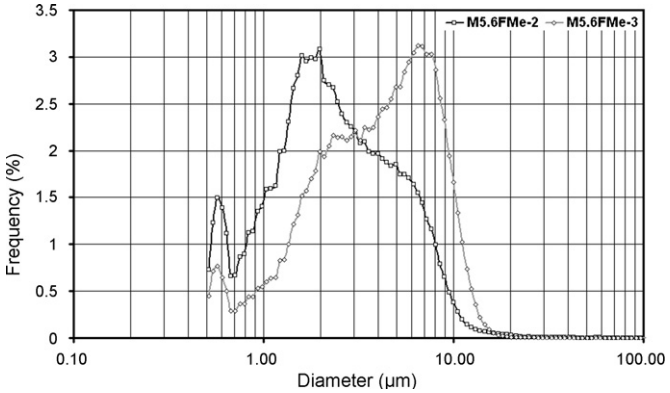

Fig. 7. Effect of stirring rate on size distribution of microcapsules for $M_{5.6}$FMe-2 and $M_{5.6}$FMe-3 samples.

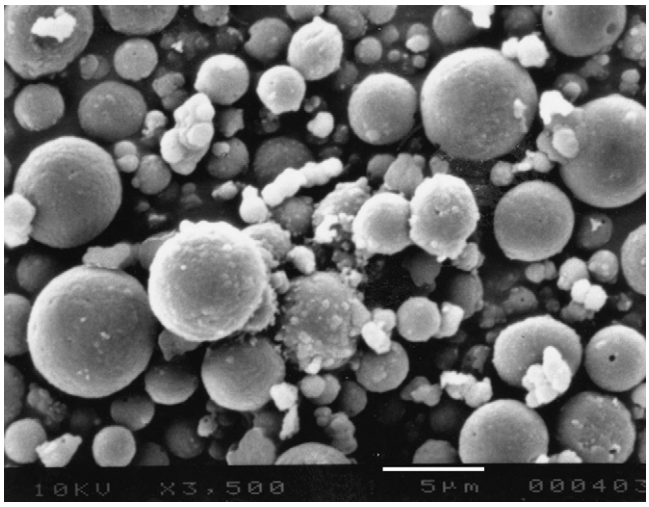

Fig. 8. SEM micrograph of $M_{5.6}$FMe-3 at a magnification of 3500.

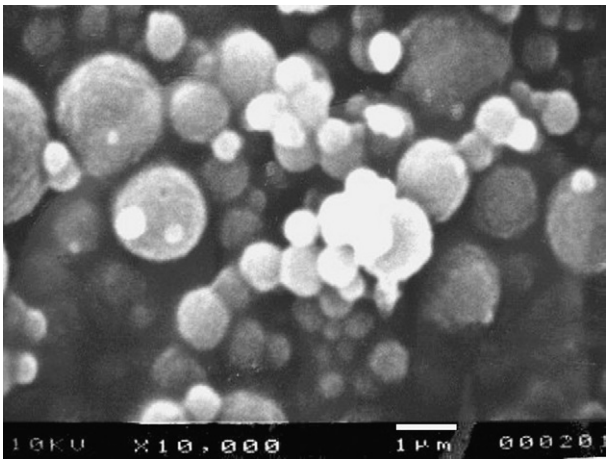

Fig. 10. SEM micrograph of M_4FMe-1 at a magnification of 10,000.

formation of higher oligomers of melamine–formaldehyde polymer with the formation of methylene bridges can be described as the reaction of bound CH_2OH group with bound NH_2 group or H.

3.2.4. Influence of the pre-polymer used as shell material

The kinetics of the shell formation and the morphology of the microcapsules are deeply influenced by the molar ratio of the pre-polymer and therefore the particle size distribution is affected. Thus, when the M–F molar ratio increases, high degree of cross-linking melamine–formaldehyde resin is obtained via the formation of ether bridges and the phase separation time decreases. As a result, the surface of the particles becomes rougher (Figs. 8 and 10). The influence of molar ratio on the particle size distribution is shown in Fig. 11. When, the molar ratio is decreased, a narrow size distribution is obtained, with a lower mean diameter. Whereas a bimodal distribution was observed for $M_{5.6}$FMe and M_6FMe, with one maximum at about 1.8 μm and another at about 8 μm. The difference in the size distribution profile can be also related to the surface activity of the pre-polymer. Thus, a lower ratio induces a higher surface activity and a lower aqueous solubility therefore the pre-polymer tend to deposit around the oily core material to stabilize the dispersed phase during the emulsion step.

3.2.5. Effects of pre-polymer amount

The effect of melamine–formaldehyde pre-polymer on the size distribution is shown in Fig. 12. The size distribution of microcapsules obtained with low concentration of melamine–formaldehyde pre-polymer appeared narrower than those obtained with higher concentration, even if they present a bimodal distribution with one peak at 3 μm and a second at 7 μm, excepted for $M_{5.6}$FMe-6 where the lower value was around 1.8 μm. When the amount of amino resin increased until 25.2 g, the distributions showed an increase in the fraction of large particles. For higher amount, the formation of tiniest microcapsules was observed. The smaller population could be satellite droplets formed during the emulsion in the presence of a surface active resin that promoted low interfacial tension. Thus, when the amount of resin increased, the resistance to

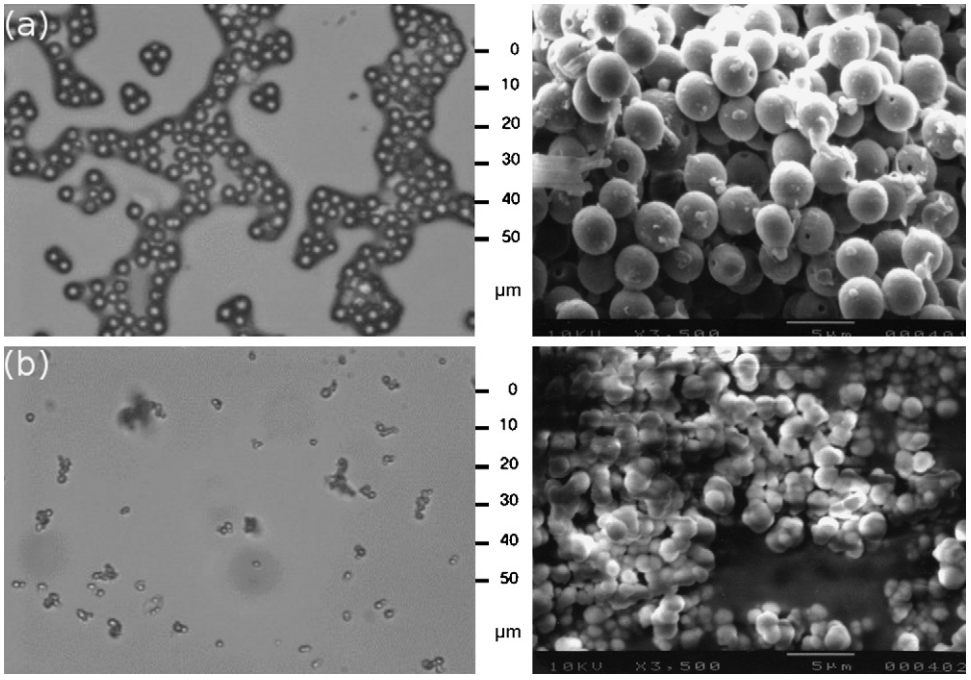

Fig. 9. Optical (×64) and SEM (×3500) micrographs of $M_{5.6}$FMe-1 and $M_{5.6}$FMe-2, respectively.

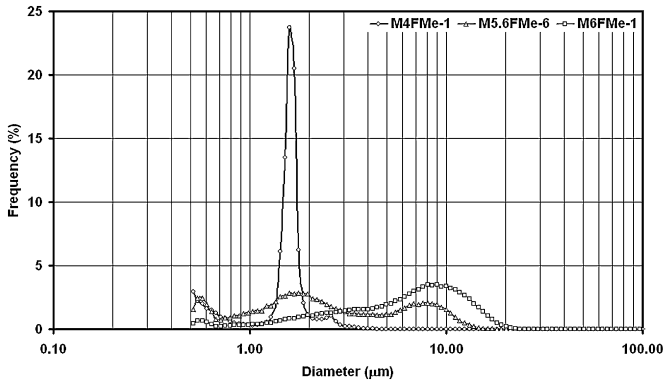

Fig. 11. Effect of molar ratio on size distribution of microcapsules for M_4FMe-1, $M_{5.6}$FMe-6 and M_6FMe-1 samples.

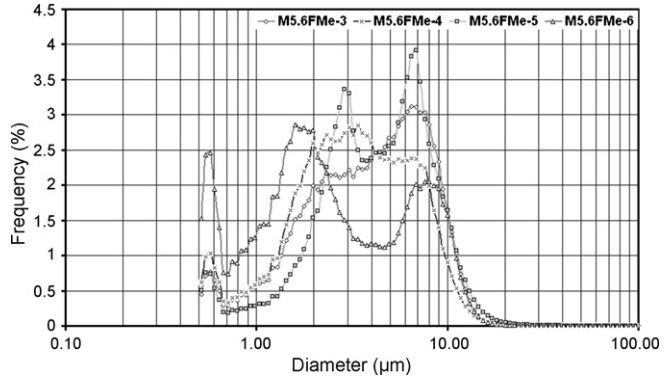

Fig. 12. Effect of melamine–formaldehyde pre-polymer concentration on the microcapsules size distribution.

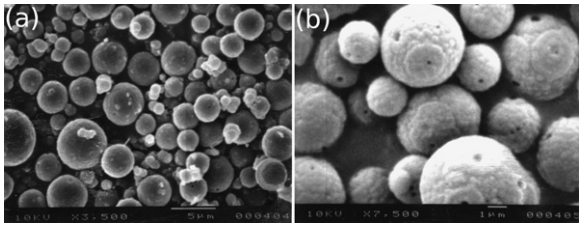

Fig. 13. SEM (×3500 and ×7500) micrographs of $M_{5.6}$FMe-4 (a) and $M_{5.6}$FMe-5 (b).

drop breakage decreased, leading to a decrease of the mean droplet size. Furthermore, higher melamine–formaldehyde resin concentration resulted in increased continuous phase viscosity (Table 1), promoting the break-up of *n*-hexadecane droplets.

From the results of the melting enthalpy, the *n*-hexadecane measured content in the microcapsules was slightly higher than the theoretical one. Thus, a part of the amino resin was not converted to the polymer shell and was dissolved in the continuous phase [27]. These oligomers could be deposited later onto the microcapsules shell during the recovery process as illustrated in Fig. 13 with the presence of dimples and fragments. Nevertheless, the higher was the amount introduced the higher was the resin conversion found (70% for $M_{5.6}$FMe-4, 82.2% for $M_{5.6}$FMe-3, 88% for $M_{5.6}$FMe-5 and 97% for $M_{5.6}$FMe-6).

4. Conclusion

Microcapsules based on *n*-hexadecane core and melamine–formaldehyde shell were synthesized via an *in situ* polymerization process. In this work, process parameters affecting either the formation of a stable emulsion or the shell formation step during the microencapsulation process were also investigated. Thus, it was found from the tensiometric measurements that the optimum emulsion conditions were obtained with a binary mixture of Tween-20 and Brij-35, a phase volume ratio of 0.42 and a pH adjusted to 4. The stirring and stirring time were adjusted to allow the formation of microcapsules with a mean diameter between 0.5 and 10 μm. It was found that, the weight ratio of the core/shell materials affected also the particle size, its distribution and the surface morphology of the microcapsules.

References

[1] D.P. Colvin, Y.G. Bryant, Fibre with reversible enhanced thermal storage properties and fabric made there from, US Patent 4 756 958 (1988).
[2] K.E. Kaska, M.M. Chen, Improvement of the performance of solar energy of waste heat utilization systems using phase change slurry as enhanced heat transfer storage fluid, J. Sol. Energy Eng. 107 (1985) 229–236.
[3] Y. Yamagishi, H. Takeuchi, A. Pyatenko, Characteristics of microencapsulated pcm slurry as a heat-transfer fluid, AIChE J. 45 (1999) 696–707.
[4] B. Pause, Development of heat and cold insulating membrane structures with phase change material, J. Coated Fabrics 25 (7) (1995) 59–68.
[5] P. Leitch, T.H. Tassinari, Interactive textiles; new materials in the new millennium. Part 1, J. Ind. Textiles 29 (3) (2000) 173–190.
[6] E. Mccullough, Phase change and protective possibilities, Ind. Fabric Prot. Rev. (2001) 64–67.
[7] Y.G. Bryant, D.P. Colvin, Fibers with enhanced, reversible thermal energy storage properties, Messe Frankf. (1992) 1–8.
[8] M.N.A. Hawlader, M.S. Uddin, H.J. Zhu, Encapsulated phase change materials for thermal energy storage: experiments and simulation, Int. J. Energy Res. 26 (2002) 159–171.
[9] M.L. Soto-portas, A.F. Argillier, F. Mechin, N. Zydowicz, Preparation of oily core polyamide microcapsules via interfacial polycondensation, Polym. Int. 52 (2003) 522–527.
[10] J.S. Cho, A. Kwon, C.G. Cho, Microencapsulation of octadecane as a phase change material by interfacial polymerization in an emulsion system, Colloid Polym. Sci. 280 (2002) 260–266.
[11] X.Z. Lan, Z.C. Tan, G.L. Zou, L.X. Sun, T. Zhang, Microencapsulation of n-eicosane as energy storage material, Chin. J. Chem. 22 (2004) 411–414.
[12] H. Yoshizawa, E. Kamio, N. Hirabayashi, J. Jacobson, Y. Kitamura, Membrane formation mechanism of cross-linked polyurea microcapsules by phase separation method, J. Microencapsulation 21 (3) (2004) 241–249.
[13] X.X. Zhang, X.M. Tao, K.L. Yick, X.C. Wang, Structure and thermal stability of microencapsulated phase-change materials, Colloid Polym. Sci. 282 (2004) 330–336.
[14] Y.F. Fan, X.X. Zhang, X.C. Wang, J. Li, Q.B. Zhu, Super-cooling prevention of microencapsulated phase change material, Thermochim. Acta 413 (2004) 1–6.
[15] Q. Song, Y. Li, J. Xing, J. Hu, Y. Marcus, Thermal stability of composite phase change material microcapsules incorporated with silver nano-particles, Polymer 48 (11) (2007) 3317–3323.
[16] K.L. Mittal, Determination of CMC of polysorbate 20 in aqueous solution by surface tension method, J. Pharm. Sci. 61 (1972) 1334–1335.
[17] M.J. Akers, V. Vasudevan, M. Stickelmeyer, Formulation development of protein dosage form, in: S.L. Neil, M.J. Akers (Eds.), Development and Manufacture of Protein Pharmaceuticals, Pharmaceutical Biotechnology, vol. 14, Kluwer Academic/Plenum Publishers, New York, 2002, pp. 47–84.
[18] D.N. Rubingh, in: K.L. Mittal (Ed.), Solution Chemistry of Surfactants, vol. 1, Plenum, New York, 1979.
[19] M.J. Rosen, Surfactants and Interfacial Phenomena, 2nd ed., Wiley-Interscience, New York, 1989.
[20] J.R. Kanicky, D.O. Shahi, Effect of degree, type, position of unsaturation on the pKa of long-chain fatty acids, J. Colloid Interface Sci. 190 (1997) 71–75.
[21] H.S. Tan, T.H. NG, H.K. Mahabadi, Interfacial polymerization encapsulation of a viscous pigment mix: emulsification conditions and particle size distribution, J. Microencapsulation 8 (4) (1991) 525–536.
[22] B.P. Binks, W.G. Cho, P.D.I. Fletcher, D.N. Petsev, Stability of oil-in-water emulsions in a low interfacial tension system, Langmuir 16 (2000) 1025–1034.
[23] W.J. Luo, W. Yang, S. Jiang, J.M. Feng, M.B. Yang, Microencapsulation of decabromodiphenyl ether by in situ polymerization: preparation and characterization, Polym. Degrad. Stab. 92 (7) (2007) 1359–1364.
[24] X.X. Zhang, Y.F. Fan, X.M. Tao, K.L. Yick, Fabrication and properties of microcapsules and nanocapsules containing n-octodecane, Mater. Chem. Phys. 88 (2–3) (2004) 300–307.
[25] K. Dietrich, E. Bonatz, R. Nastke, H. Herma, M. Walter, W. Teige, Amino resin microcapsules. IV. Surface tension of the resins and mechanism of capsule formation, Acta Polym. 41 (2) (1990) 91–95.
[26] H.Y. Lee, S.J. Lee, I.W. Cheong, J.H. Kim, Microencapsulation of fragrant oil via in situ polymerization: effects of pH and melamine–formaldehyde molar ratio, J. Microencapsulation 19 (5) (2002) 559–569.
[27] K. Dietrich, E. Bonatz, H. Geistlinger, H. Herma, R. Nastke, H.J. Purz, M. Schlawne, W. Teige, Amino resin microcapsules II Preparation and morphology, Acta Polym. 40 (5) (1989) 325–331.